RESEARCH ARTICLE

Characteristics and turnover of exopolymeric substances in a hypersaline microbial mat

Olivier Braissant[1], Alan W. Decho[2], Kristen M. Przekop[1], Kimberley L. Gallagher[1], Christina Glunk[3], Christophe Dupraz[1] & Pieter T. Visscher[1]

[1]Center for Integrative Geosciences, University of Connecticut, Storrs, CT, USA; [2]Arnold School of Public Health, University of South Carolina, Columbia, SC, USA; and [3]Institut de Géologie et d'Hydrogéologie, University of Neuchâtel, Neuchâtel, Switzerland

Correspondence: Pieter T. Visscher, Center for Integrative Geosciences, University of Connecticut, U-2045, Storrs, CT 06269-2045, USA. Tel.: +1 860 405 9159; fax: +1 860 405 9153; e-mail: pieter.visscher@uconn.edu

Received 5 June 2008; revised 28 August 2008; accepted 17 September 2008.
First published online 27 November 2008.

DOI:10.1111/j.1574-6941.2008.00614.x

Editor: Patricia Sobecky

Keywords
exopolymeric substances (EPS); microbial mat; calcium carbonate precipitation; glucosidase activity.

Abstract

The properties and microbial turnover of exopolymeric substances (EPS) were measured in a hypersaline nonlithifying microbial mat (Eleuthera, Bahamas) to investigate their potential role in calcium carbonate ($CaCO_3$) precipitation. Depth profiles of EPS abundance and enzyme activities indicated that *c.* 80% of the EPS were turned over in the upper 15–20 mm. Oxic and anoxic mat homogenates amended with low-molecular-weight (LMW) organic carbon, sugar monomers, and different types of EPS revealed rapid consumption of all substrates. When comparing the consumption of EPS with that of other substrates, only marginally longer lag times and lower rates were observed. EPS (5–8%) were readily consumed during the conversion of labile to refractory EPS. This coincided with a decrease in glucosidase activity and a decrease in the number of acidic functional groups on the EPS. Approximately half of the calcium bound to the EPS remained after 10 dialyses steps. This tightly bound calcium was readily available to precipitate as $CaCO_3$. We present a conceptual model in which LMW organic carbon complexed with the tightly bound calcium is released upon enzyme activity. This increases alkalinity and creates binding sites for carbonate and allows $CaCO_3$ to precipitate. Therefore, this model explains interactions between EPS and $CaCO_3$ precipitation, and underscores the critical role of aerobic and anaerobic microorganisms in early diagenesis and lithification processes.

Introduction

In many environments, microorganisms are associated with biofilms, which are comprised of exopolymeric substances (EPS) (Sutherland, 2001a). By producing these EPS, microorganisms engineer their immediate environment with respect to many physicochemical characteristics (Costerton *et al.*, 1987, 1995). The EPS are mainly comprised of polysaccharides, but also include noncarbohydrate moieties such as pyruvate and succinate, as well as inorganic functional groups such as sulfate or phosphate (Sutherland, 2001a–d). In microbial mats, which are organosedimentary biofilm communities and analogs of the earliest life on Earth (Riding & Awramik, 2000), the EPS provide an important cohesive matrix where many biogeochemical reactions take place (Stal *et al.*, 1985; Stolz, 2000). In siliciclastic environments, the physical properties of the gel-like cohesive matrix of the EPS may produce microbially induced sedimentary structures, or MISS (Noffke *et al.*, 2003), which are preserved in the rock record (Tice, 2008). However, in carbonate sediments forming modern stromatolites, the focus has been on the chemical properties of the EPS (Kawaguchi & Decho, 2002a, b). Notably, the functional groups within the EPS produced by microbial isolates from microbial mats and biofilms have a high affinity for calcium and other metals (Perry *et al.*, 2005; Braissant *et al.*, 2007; Ortega-Morales *et al.*, 2007). As a consequence, even under slightly supersaturated conditions with respect to calcium carbonate ($CaCO_3$), this cation-binding capacity may initially inhibit $CaCO_3$ precipitation (Braissant *et al.*, 2007). It has been hypothesized that $CaCO_3$ precipitation requires sequential

heterotrophic bacterial degradation of EPS to release calcium and increase carbonate alkalinity (Dupraz & Visscher, 2005).

Several studies have focused on degradation of EPS (Sutherland, 1995, 1999; Hashimoto *et al.*, 1998; Nankai *et al.*, 1999), but few have been carried out in natural systems. Experiments using $H^{14}CO_3^-$ to label cyanobacterial EPS in intact stromatolites suggest that the labile part of this freshly produced polymer is rapidly modified by heterotrophic bacteria to leave a more refractory polymer (Decho *et al.*, 2005). This refractory material accumulates in the environment, where it is subject to very slow chemical modification and microbial breakdown. When added to marine sediment and lacustrine water samples, ^{14}C-labeled EPS was also degraded rapidly (Henrichs & Doyle, 1986; Weaver & Hicks, 1995). Moreover, all of these studies recovered only a fraction of the labeled polymers as $^{14}CO_2$ (10–40%; i.e. representing the labile fraction), suggesting that the remaining polymer is more resistant to degradation. The amendment of xanthan, a commercially produced EPS, to marine sediment slurries enhanced the activity of sulfate-reducing bacteria [SRB; Battersby *et al.* (1984)]. This stimulation was attributed to a combination of initial xanthan degradation by fermenters releasing low-molecular-weight (LMW) organic acids and alcohol (Anderson *et al.*, 1987).

The degradation of EPS will alter its physicochemical properties such as pH buffering and calcium binding, thereby influencing $CaCO_3$ precipitation processes in mats. This study focuses on the amount, the characteristics, and distribution of the natural EPS in a hypersaline microbial mat that supports $CaCO_3$ precipitation. In order to investigate the role of EPS in precipitation, in this study, we chemically characterized EPS properties by acid–base titrations, X-ray photoelectron spectroscopy (XPS), and Fourier-transform infrared (FT-IR) spectroscopy. The degradation of EPS was studied using hydrolytic enzyme activities and slurries, and the potential of EPS as a calcium source to support carbonate mineral precipitation was investigated in biomineralization experiments (Braissant *et al.*, 2003; Ercole *et al.*, 2007).

Materials and methods

Site description

Salt Pan (76°33′W, 25°24′N) is a hypersaline lake, located 3 km north of Gregory Town, Eleuthera, Bahamas (Fig. 1), which supports a gradient of lithifying, EPS-poor to nonlithifying, EPS-rich microbial mats (Dupraz *et al.*, 2004). Both mat types are always submerged, but the lithifying mats are found close to the shoreline (maximum water depth 30 cm), whereas the nonlithifying mats are found in the center of the lake, where the water is deeper (30–75 cm depth). There is an abrupt transition from the zone of lithifying to the zone of nonlithifying mats, possibly determined by the light regime (Dupraz *et al.*, 2004). The microbial communities in the mats were described previously (Baumgartner, 2006; Baumgartner *et al.*, 2006). The salinity varies between 40 and 150 p.p.t., and the pH ranges from 8 to 9. The water temperature averages are 22 and 30 °C, in winter and in summer, respectively (Baumgartner, 2006). The water column in this lake is well mixed due to wind-driven circulation and diel thermal turnover of the water column. The maximum light intensity ranges from 38–88 $\mu E\,m^{-2}\,s^{-1}$ at the surface of the nonlithifying mats to 112–193 $\mu E\,m^{-2}\,s^{-1}$ at the surface of the lithifying mats. The lithifying mats contain only a thin film (i.e. less than a millimeter) of EPS on top of the crust. The EPS extraction and purification procedures used in this investigation did not yield sufficient amounts of EPS for the analyses. Therefore, in this study, we focused on the EPS-rich nonlithifying systems.

Geochemical properties of nonlithifying mats

Nonlithifying mat samples were taken about 25 m from the shore, where the water depth was about 40 cm. The intensity of photosynthetically active radiation was measured with a Licor LI-250 meter equipped with an underwater quantum sensor (LI-192). The salinity was determined using a hand-held refractometer (Fisher Scientific) and the water temperature and pH were determined using a hand-held meter (Hannah HI 9024). The mat samples were incubated at

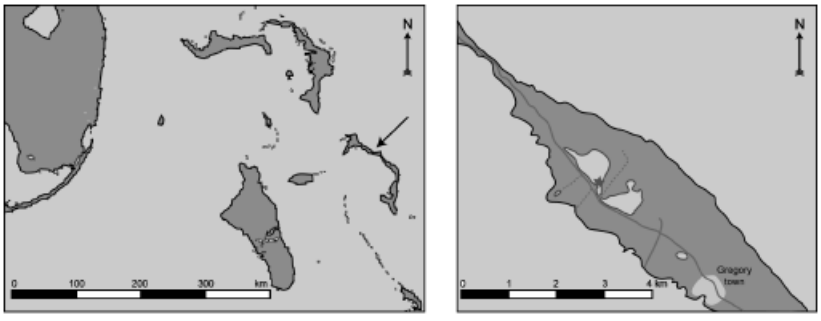

Fig. 1. Sampling site location of Salt Pan, Eleuthera, Bahamas.

ambient light (*c.* 0–90 μE m^{-2} s^{-1} during a diel cycle) using a neutral density screen to simulate the light attenuation of the water column. The salinity (90 p.p.t.), temperature (20–27 °C), and pH (8.1) of the overlying water were also maintained at near-ambient values. The following day, the depth profiles of oxygen were measured using polarographic sensors (Visscher *et al.*, 1991) equipped with a guard cathode (tip diameter 60 μm; Unisense, Denmark). The signal was registered with a picoammeter (Unisense PA2000), and the oxygen concentration was calculated from laboratory and field calibrations. Electrodes were mounted on a hand-driven micromanipulator (Märzhäuser, Wetzlar, Germany), and the oxygen concentration was measured in the top 20 mm in 250 μm increments. Profile measurements were replicated four times.

EPS extraction and purification

The upper 4 cm of nonlithifying microbial mats were dissected into 0.5–1 cm layers. The EPS extraction protocol was based on previously described extractions of mat samples (Decho *et al.*, 2003). The layers were homogenized in 100 mM EDTA (1 L EDTA kg^{-1} mat) while being stirred gently for 3–4 h. The samples were then centrifuged (15 000 ***g***, for 20 min) to remove the remaining particles. These unfiltered samples were used to determine the amount of EPS in the mats.

Samples used for acid–base titrations, the calcium-binding assay, XPS, and FT-IR were recovered from the top layer (i.e. upper 2 cm of the mat, i.e. the cyanobacterial layer) and the bottom layer (i.e. below 2 cm depth). EPS used as a carbon source in slurry experiments were recovered from the top 2 cm. Samples were sequentially filtered using 100, 1, and 0.2 μm pore sizes. The filtrate was precipitated using three volumes of 4 °C ethanol per volume of filtrate. The precipitate was recovered by centrifugation (3000 ***g***, 5 min), placed in dialysis tubing (10–12 kDa), and dialyzed against deionized water (> 18 MΩ). Samples used for the calcium-binding assay were dialyzed nine times additionally: three times for 6 h against 1 mM EDTA (pH 8.0), three times using 0.5% acetic acid, and three times with deionized water, respectively. After dialysis, the EPS was stored at 4 °C or freeze-dried.

Physicochemical properties and abundance of EPS

EPS depth profiles

The quantity of EPS with depth in the microbial mat was estimated using two different assays: the phenol–sulfuric acid assay (Dubois *et al.*, 1956) and the Alcian Blue assay (Passow & Alldredge, 1995; Bober *et al.*, 2005). The phenol–sulfuric acid method determines the amount of reducing sugars constituting EPS upon hydrolysis, whereas Alcian Blue assays for EPS based on the presence of anionic functional groups. Therefore, these two assays are complementary.

Unfiltered EPS samples were diluted 10 times in 90 p.p.t. water, and 6 mL of cold ethanol was added to precipitate the EPS. Subsequently, the samples were centrifuged (3000 ***g***, 20 min) and the pellets were used for either of the two assays. For the phenol–sulfuric acid assay, the wet pellets were resuspended into 300 μL of water, after which 50 μL of 80% phenol was added. Finally, 2 mL of concentrated sulfuric acid was added. The samples were allowed to cool to room temperature, and the absorbance of the solution was measured at 490 nm. For the Alcian Blue assay, the pellet was air dried for 1 h. Two milliliters of 0.15 mg mL^{-1} Alcian Blue 8GX was added in 5% acetic acid. The mixture was allowed to react for 1 h, centrifuged (3000 ***g***, 20 min), and the absorbance of the supernatant was read at 614 nm. Two replicates were used in both assays. For both assays, xanthan solutions were used as a standard.

XPS

XPS analyses were performed to measure the elemental composition of the EPS (Omoike & Chorover, 2004; Ortega-Morales *et al.*, 2007), using a Phi Multiprobe system (Chanhassen, MN). Dialyzed EPS samples from the top and the bottom layers were mounted on stainless-steel stubs using a copper tape and allowed to air dry. The samples were analyzed using a nonmonochromatized Al X-ray source (Anode voltage 15 kV, emission current 13 mA). A 45° emission angle was used for all samples.

FT-IR spectroscopy of EPS

FT-IR spectroscopy was used to determine the presence of specific functional groups within the EPS (Raguénès *et al.*, 1996, 2004; Braissant *et al.*, 2007) such as carboxyl, sulfate, sulfinic acids, thiols, hydroxyl, and amino groups of purified EPS (Smith, 1996). EPS was purified by precipitation in ethanol and dialysis as described above. Fresh mat samples were collected on Eleuthera, Bahamas, and natural EPS was immediately extracted and purified as described above for analysis. Analyses were conducted on a Nexus 670 FT-IR spectrometer equipped with attenuated total reflectance and fitted with a multibounce germanium crystal (Thermo-Nicolet Inc., Madison, WI). Dry EPS samples (*c.* 1 mg) were placed in a Thunderdome Tilt-back Pressure Tower (Spectro-Tech Foundation Series, Thermo-Nicolet Inc.), which is designed to achieve optimal contact between the sample and the crystal. This provides an active sampling area of *c.* 0.75 mm, with an effective path length of 2.03 μm at 1000 cm^{-1} [assuming an average index of refraction (for a sample) of 1.5 and an angle of incidence of 45°]. Absorbance

spectra were collected between 4000 and 600 cm^{-1} at a spectral resolution of 4 or 8 cm^{-1}, with 64 scans coadded and averaged. If necessary, baseline corrections were carried out.

Acid–base titration

The acid–base titration was used to determine the proton-binding sites and the potential types and densities of the functional groups present in the EPS. For the acid–base titration, 2–3 mL of the dialyzed EPS (*c.* 6.5 mg of dry EPS) were diluted in 1 mM KCl to obtain a final volume of 40 mL. KCl was used to adjust ionic strength. The solution was transferred to an anaerobic chamber (COY Laboratory Product, Grass Lake, MI) under a nitrogen (98%)–hydrogen (2%) atmosphere to avoid the dissolution of atmospheric CO_2. The initial pH of the solution was adjusted to 3.0, which typically required between 30 and 100 μL of 1 N HCl. The solution was titrated with 0.1 N NaOH using 10 μL increments. The pH was recorded with an Orion 720A pH meter (Orion, Boston, MA) until a pH of 11 was reached. All reagents were prepared with autoclaved deionized water that was cooled to room temperature under vacuum to remove all dissolved CO_2. The titration curves obtained were analyzed using PROTOFIT 2.1 software (Turner & Fein, 2006). For the analysis, we assumed a four-site, nonelectrostatic model as recommended for biological surfaces (Turner & Fein, 2006).

Calcium assay

The calcium chloride ($CaCl_2$) assay was carried out to establish the maximum calcium-binding capacity of the EPS. This titration was performed according to Shimomura & Inouye (1996) under a nitrogen (98%)–hydrogen (2%) atmosphere to avoid ion pairing of calcium with carbonate resulting from atmospheric CO_2 dissolution. Dialyzed EPS samples were dissolved in a solution containing 40 mM KCl and 20 mM Tris-OH, which was adjusted to pH 9.0. The titration was carried out by stepwise addition of a $CaCl_2$ solution (0.1 or 1 M) using increments of either 10 or 40 μL. The concentration of free calcium ions was determined with a calcium ion-selective electrode (Cole-Palmer Instruments, Vernon Hills, IL) and a calomel reference electrode (Fisher Scientific) coupled to a high-impedance millivolt meter (Microscale Measurement, the Netherlands). All reagents were prepared using autoclaved deionized water that was allowed to cool to room temperature under vacuum.

Microbial potential of EPS degradation

Reductase activity assay

The reduction of triphenyltetrazolium chloride (TTC) to triphenylformazan is used as a measure of the total reductase activity in microbial populations (Relexans, 1996) and has been applied to microbial mats (Paerl *et al.*, 2001). Mat samples (2 g) were homogenized and mixed with 2 mL of 0.8% TTC, prepared in 0.1 M Tris buffer containing 600 mM NaCl at pH 7.6. The samples were incubated for 1–3 h at 30 °C with periodic shaking. Following the incubation, the samples were centrifuged (3000 ***g***, 10 min) and the pellet was resuspended in 10 mL of acetone to extract the triphenylformazan. After 15 min, the concentration of formazan that was produced was measured spectrophotometrically at 490 nm. The Beer–Lambert law was used to calculate the concentration of formazan [molar absorption coefficient, $\varepsilon_{490} = 15\,900\ L\ mol^{-1}\ cm^{-1}$, Relexans (1996)] released. The assay was performed using 12 replicates, and blanks were prepared using samples fixed in glutaraldehyde 1.5% (final concentration), which were subjected to the same treatment.

Hydrolytic enzymes assay

Microbial degradation of EPS may be facilitated through hydrolytic enzyme activity (Hashimoto *et al.*, 1998; Nankai *et al.*, 1999). To measure the hydrolytic activity of α-glucosidase, β-glucosidase, and β-galactosidase, 2 g of homogenized mat samples were placed to 3 mL of Z-buffer (600 mM NaCl, 60 mM Na_2HPO_4, 40 mM $NaH_2PO_4 \cdot H_2O$, 10 mM KCl, 1 mM $MgSO_4 \cdot 7H_2O$, and 2 mM β-mercaptoethanol, pH 7.0) to which 50 μL of sodium dodecyl sulfate 0.1% and 100 μL of chloroform were added. The tubes were shaken vigorously and allowed to react for 5 min. Subsequently, 200 μL of substrate (13 mM *o*-nitrophenyl-β-D-galactoside, 13 mM *o*-nitrophenyl-β-D-glucoside, and 13 mM *o*-nitrophenyl-α-D-glucoside) was added and the samples were incubated at 30 °C, while being shaken periodically. After 5–8 h, samples were centrifuged (3000 ***g***, 10 min) and the absorbance of the supernatant was measured at 420 nm. The Beer–Lambert law was used to calculate the concentration of *o*-nitrophenol [molar absorption coefficient, $\varepsilon_{420} = 4580\ L\ mol^{-1}\ cm^{-1}$, Stolle-Smits *et al.* (1999)] released and consequently the activity. Three, three, and nine replicates were used for the α-glucosidase assay, β-glucosidase, and β-galactosidase, respectively. Blanks were prepared using samples fixed in glutaraldehyde 1.5% (final concentration), which were subjected to the same treatment.

Slurry experiments

Microbial mats were homogenized to determine the potential respiration rates supported by a range of electron donors (Visscher *et al.*, 1998, 1999, 2002; Decho *et al.*, 2005). We compared slurries prepared from lithifying and nonlithifying mats and measured the potential EPS turnover under oxic and anoxic conditions in relation to other electron donors. Nonlithifying mat slurries were prepared from

0–10 mm to 30–40 mm horizons, for top and bottom slurries, respectively. Lithifying mat slurries were prepared from the entire (*c.* 10 mm) mat sample. Sediments were mixed (1 : 1 v/v) with filtered seawater amended with NaCl to 90 p.p.t. The slurries were preincubated for 24–36 h to remove labile carbon, after which the endogenous respiration rates were determined. Aerobic respiration rates were measured as the oxygen consumption over time using an oxygen microelectrode and anaerobic respiration as the sulfide production over time using a sulfide microelectrode (Visscher *et al.*, 1998, 2002). Sulfide production results from sulfate reduction, which is considered the dominant anaerobic pathway in mats (Troelsen & Jørgensen, 1982; Canfield & DesMarais, 1991; Baumgartner *et al.*, 2006). Slurry aliquots completely filled a 36-mL gas-tight incubation vessel under stirred conditions. Electron donors (acetate, lactate, ethanol, glucose, mannose, and xylose) were supplied at final concentrations of 69 μM, and the exopolymers used included xanthan, EPS isolated from *Desulfobacterium autotrophicum*, EPS isolated from a *Desulfovibrio* strain LM-1 isolated from the lithifying mat of Salt Pan (Braissant *et al.*, 2007), and nonlithifying mat EPS from the surface 20 mm. The EPS amendments equaled *c.* 20 μg of EPS. All of the rate measurements were corrected for the endogenous respiration rates. The amount of carbon oxidized was estimated from the oxygen consumed (or S^{2-} produced) using an average oxidation state of zero for carbon, according to

$$CH_2O + O_2 \rightarrow CO_2 + H_2O \quad (1)$$

and

$$2CH_2O + SO_4{}^{2-} \rightarrow 2CO_2 + S^{2-} + 2H_2O, \quad (2)$$

respectively. All slurry amendments were replicated three to five times.

Carbonate mineral precipitation potential of EPS

Biomineralization experiments were conducted to determine whether calcium bound to the EPS could support $CaCO_3$ precipitation. Previous studies indicated that a large amount of cations (especially calcium and magnesium) remain associated with natural EPS even after several dialysis steps (Somers & Brown, 1978). Therefore, no cations were added in the solution for this experiment. Dialyzed EPS was placed in six-well plates (3 mg in each well), and deionized water was added to a final volume of 4 mL. The plate was placed in a closed desiccator containing 5 g of $(NH_4)_2CO_3$. Slow decomposition of the $(NH_4)_2CO_3$ into CO_2 and NH_3 and further dissolution of these gases into the EPS solution led to an increase in pH and to formation of carbonate ions and subsequent precipitation of minerals. The precipitation reaction was allowed to proceed for 5 days. The crystals formed were recovered by filtration. To prevent the recrystallization of ammonium carbonate, filters were rapidly washed with 0.2 mL of DI water (pH adjusted to 9.5 to prevent $CaCO_3$ crystal dissolution). A part of the filter was cut and mounted on a specimen holder, sputtered with gold, and observed in a LEO/Zeiss DSM 982 Gemini field emission scanning electron microscope (SEM). Xanthan, used as a calcium-free control, did not support precipitation after 5 days of incubation.

Results

Geochemical depth profiles in nonlithifying mats

The oxygen concentration increased with depth and peaked at 4–6 mm below the mat surface. The observed maximum values corresponded with *c.* 160–170% saturation, which confirmed earlier observations made at the opposite side of the lake (Dupraz *et al.*, 2004). A typical oxygen depth profile is given in Fig. 2c. The depth of oxygen penetration was 16–19 mm, which suggested that aerobic respiration could take place until this depth. The majority of the enzyme activities were also associated with this layer.

Physicochemical properties and abundance of EPS

The amount of EPS in the mat measured by the phenol–sulfuric acid assay showed a relatively constant distribution in the top 15 mm [*c.* 10^4 μg EPS g^{-1} dry weight (DW) sediment], after which it decreased fivefold (Fig. 2a). The values determined by the Alcian Blue method increased from 7.7×10^3 μg EPS g^{-1} DW at the surface to a peak at the 10–15 mm horizon (2.25×10^4 μg EPS g^{-1} DW), and decreased to a third at deeper layers (Fig. 2b).

XPS

XPS analyses of the top and bottom EPS layers showed a very similar elemental composition of the two depth horizons (Fig. 3 and Table 1): C, O, N, and S were present in similar atomic percentages. In addition, both XPS spectra showed a calcium peak, which indicated that calcium represents *c.* 1% of the total atoms in the EPS. The C : O ratio increased from 2.19 in the top layer to 2.33 in the bottom layer of the EPS. This increase with depth, although minor, may be indicative of an early stage in the degradation (i.e. kerogenization) process.

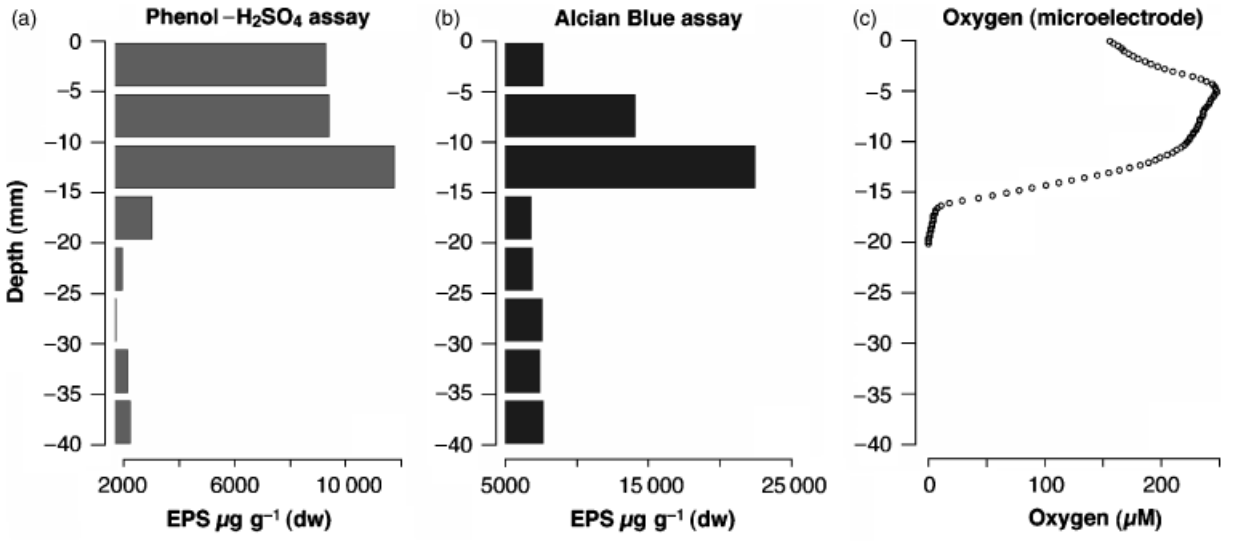

Fig. 2. Depth profiles of EPS in the microbial mat determined with the phenol–sulfuric acid assay (a) and the Alcian Blue assay (b), respectively. Depth profile of oxygen measured during peak photosynthesis at 12:30 hours (c) indicating the depth of the oxic zone.

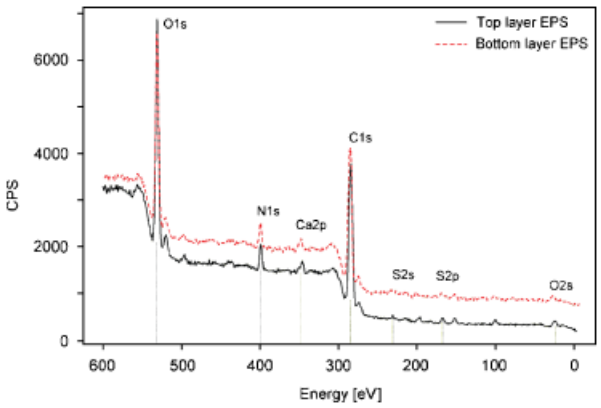

Fig. 3. XPS of top (0–20 mm) layer EPS (solid line) and bottom (20–40 mm) layer EPS (dashed line). Note the presence of the calcium peak in both spectra at 350 eV.

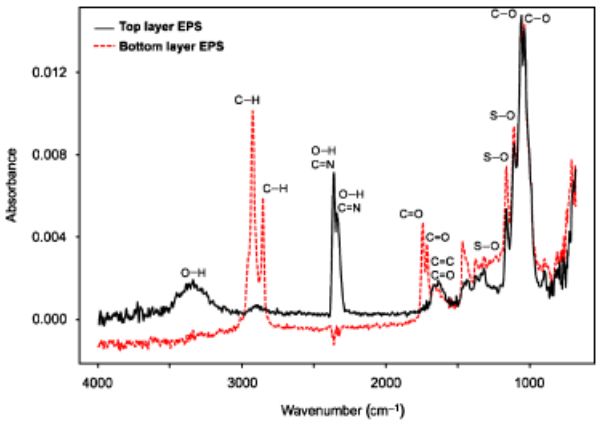

Fig. 4. FT-IR spectra of top (0–20 mm) layer EPS (solid line) and bottom (20–40 mm) layer EPS (dashed line). Note the large quantity of O–H bonds in top layer EPS (only a small peak is present in bottom layer EPS). In contrast, the bottom layer EPS has a greater abundance of C–H bonds compared with the top layer. Also note the differences in the presence of C=O bonds (abundant in bottom layer EPS) indicating carboxylic functional groups.

Table 1. Elemental composition of EPS from natural mats obtained by XPS

Element	Top layer EPS	Bottom layer EPS
C	63.9%	64.8%
O	29.1%	27.8%
N	5.0%	5.4%
S	1.0%	1.1%
Ca	1.0%	1.0%
C : O	2.19	2.33
C : N	12.52	12.00

The Top layer EPS represents the 0–20 mm horizon, and the bottom layer EPS was obtained from 20 to 40 mm.

FT-IR spectroscopy of EPS

FT-IR analyses (Fig. 4) showed that the extractable EPS contained several major infrared absorption peaks. Absorption peaks at 1034 and 1055 cm^{-1} were assigned to carbohydrate C–O stretching vibrations. A peak at 1108 cm^{-1} could be attributed to S=O stretching vibration from sulfate, sulfinic, or sulfonic acid (Coates, 2000; Socrates, 2001). In addition, the presence of sulfates was also indicated by the

covalent sulfate peaks at 1161 cm^{-1}, representing an S–O stretch accompanied by a deformation at 610 cm^{-1}, and a peak at 1315 cm^{-1}. The peak at 1650 cm^{-1} was likely due to C=C stretching vibrations, which exist in a vinylidene (i.e. 2H on the same C) conformation (890 cm^{-1}). The peak at 1650 cm^{-1} can also be attributed to the C=O bond typical of carboxylic groups, as they typically form a prominent peak near 1630–1650 cm^{-1}. Peaks at 1710 and 1741 cm^{-1} were likely due to carboxylic acids as well, as they are often encountered in dicarboxylic acids and ketoacids (Coates, 2000; Socrates, 2001). A doublet at 2340 and 2360 cm^{-1} could be attributed to the O–H stretching vibrations from sulfinic or sulfonic acids or alternatively to C=N bonds (Coates, 2000; Socrates, 2001). Peaks at 2853 and 2923 cm^{-1} represented C–H stretches, and 3340 cm^{-1} represented O–H stretches. Proteins were not detected using the bicinchoninic acid assay (Smith *et al.*, 1985) in dialyzed EPS samples from either top or bottom layers (data not shown). Therefore, it is unlikely that the 2853 and 2923 cm^{-1} peaks indicated amides associated with proteins. Finally, the absorption peak at 898 cm^{-1} could be attributed to the β-glycoside linkage between sugar monomers.

Strong variations in the O–H bonds (observed at 3340, 2340, and 2360 cm^{-1}) and in the C–H bonds (observed at 2853 and 2923 cm^{-1}) were found between the EPS of the top layer and the bottom layer (Fig. 4). Similar to our interpretation of the XPS results, these variations were indicative of an early diagenetic alteration (kerogenization) of EPS: the FT-IR spectra clearly showed the loss of alcohol and sulfinic/sulfonic acid groups, and a more aliphatic nature of the EPS in bottom samples, indicated by an increase of the C–H bonds. Surprisingly, the bottom layer EPS contained large amounts of carboxylic acid groups, typically characteristic for freshly produced EPS. This increase in carboxylic acids was supported by the titration data.

Acid–base titration

The titration curves for the EPS extracted from the top and bottom layers were similar (Fig. 5a and b). Nevertheless, the adsorbent (i.e. EPS) buffer function showed differences between the two layers. The adsorbent buffer function amplifies the 'signal' of the titration data, and therefore allows observation of buffering effects that are not obvious from the raw titration data. Although the EPS in both layers had a similar proton-binding capacity (Table 2), the distribution of the H^+-binding sites over the different pK values differed. The EPS from the top layer showed an increased buffering capacity below pH 2.5 when compared with the EPS from the bottom layer. Different amounts of sulfate groups, with pK values below 2.5 (Schiewer, 1999), or a different carboxylic acid content, with pK between 1.0 and 5.0 (Stumm & Morgan, 1996) could explain this observed

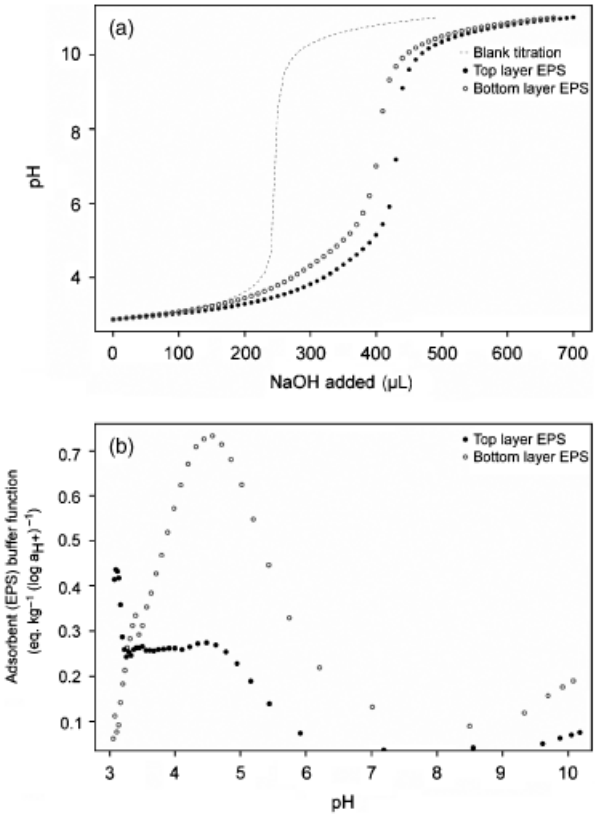

Fig. 5. Acid–base titration curve of top (●) and bottom (o) layer EPS. (a) Measured titration curve and (b) EPS buffer function computed with PROTOFIT® (Turner & Fein, 2006).

Table 2. Estimated dissociation constants (pK) for various functional groups present on top (0–20 mm) and bottom (20–40) layer EPS samples obtained by acid–base titration

EPS sample	pK_1/SD_{pk1}	pK_2/SD_{pk2}	pK_3/SD_{pk3}	pK_4/SD_{pk4}	PK_5/SD_{pk5}
Top	2.34/1.32	4.46/0.43	5.52/0.10	–	10.17/0.12
Bottom	–	4.14/0.60	4.74/0.79	6.01/0.31	10.01/0.31
	Sulfates	Carboxylic acids	Carboxylic acids	Sulfinic acids	Amino
				Sulfonic acids	Hydroxyl

shift in pK to a lower value. In contrast, the bottom layer EPS showed a higher buffering capacity between pH 4.1 and 4.7 than the top layer EPS. A different content of carboxylic acids, with pK values in the 4–5 range in the bottom layer EPS, was a possible explanation for this observation. Finally, for both the top and the bottom layer EPS, weak buffering capacities were encountered between pH 5.5 and 6.0, and at pH values higher than 10.0. These two buffering capacities were attributed to sulfinic/sulfonic acids and to amino or phenol groups, respectively (Stumm & Morgan, 1996). Although the presence of phosphate groups could also

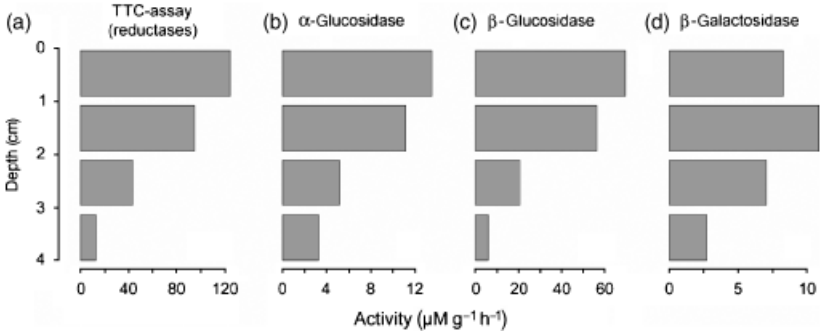

Fig. 6. Depth distribution of enzymes activities in the top 40 mm of the microbial mat. (a) Total reductase activities (TTC assay; $n = 12$); (b) α-glucosidase activity ($n = 3$); (c) β-glucosidase activity ($n = 3$); and (d) β-galactosidate activity ($n = 9$).

account for the pH 5.5–6.0 buffering, no phosphorous peaks were observed by XPS.

Calcium assay

The calcium titration indicated that the maximum binding capacities of the top and bottom layer EPS were 38 and 32 g kg^{-1}, respectively. As outlined above, the XPS analyses (Fig. 3; Table 1) revealed that both the top and the bottom layer EPS still contained *c.* 1.0 at.% of calcium (i.e. *c.* 28 g kg^{-1}) after 10 dialysis cycles. This was confirmed by atomic absorption spectroscopy, which showed that as much as half of the calcium remained in SRB-derived EPS after extensive dialysis (K. Gallagher, pers. commun.). When the XPS-derived calcium value was added, the binding capacities were 66 and 60 g kg^{-1}, in the top and the bottom layers, respectively.

Microbial potential for EPS degradation

Reductase activity

The TTC assay was used to estimate the microbial activity in the mat based on the total dehydrogenase (i.e. reductase) activities. In this study, the dehydrogenase activities showed a strong decrease with depth (Fig. 6a). The combined dehydrogenase activities in the surface 10 mm of the mat were 0.12 mM g^{-1} h^{-1} and decreased to 0.012 mM g^{-1} h^{-1} in the 30–40 mm layer.

Hydrolytic enzymes assay

Hydrolytic enzymes were used as a proxy for EPS degradation because these extracellular enzymes are required for splitting the sugar polymer into smaller fragments, including monomers, dimers, trimers, etc. For the hydrolytic enzymes assayed, β-glucosidase displayed the highest activity, decreasing with depth from 70 μmol g^{-1} h^{-1} at the top of the mat to 6 μmol g^{-1} h^{-1} at the bottom of the mat (Fig. 6b). The α-glucosidase activities (14 and 3 μmol g^{-1} h^{-1} at the top and the bottom of the mat, respectively) were

Table 3. Oxygen consumption and sulfide production in microbial mat homogenates determined upon amendment of various electron donors

	$dO_2/dt \pm SD$ (μM min^{-1})	*n*	Cox (μmol)	Lag time (min)
TOP layer aerobic respiration				
Endogenous	7.3 ± 0.9	5	0.83	0.00
Acetate	23.6 ± 2.7	4	2.48	0.25
Lactate	20.5 ± 3.4	4	3.72	0.50
Ethanol	24.1 ± 4.6	3	2.48	0.25
Glucose	34.4 ± 3.6	3	7.44	0.75
Xylose	31.6 ± 3.8	3	6.82	1.00
Mannose	34.5 ± 4.0	3	6.23	0.75
Site EPS	13.1 ± 2.1	4	1.13	1.75
D. autotrophicum EPS	4.4 ± 0.8	3	0.43	3.75
Xanthan	3.4 ± 0.6	3	0.34	3.00
Desulfovibrio EPS	8.3 ± 1.3	4	0.94	3.00
Bottom layer aerobic respiration				
Endogenous	6.4 ± 0.8	5	0.66	0.00
Acetate	25.7 ± 2.5	4	2.48	0.00
Lactate	20.5 ± 1.1	4	3.72	0.00
Ethanol	24.1 ± 4.6	3	2.48	0.00
Glucose	30.8 ± 1.7	3	6.82	0.75
Xylose	28.7 ± 1.3	3	6.82	1.00
Mannose	27.1 ± 1.3	3	6.23	1.00
Site EPS	11.8 ± 1.2	4	1.08	2.00
D. autotrophicum EPS	4.7 ± 1.7	3	0.67	4.00
Xanthan	3.0 ± 1.2	3	0.26	3.50
Desulfovibrio EPS	11.9 ± 1.7	4	1.42	3.25
	$dH_2S/dt \pm SD$ (μM min^{-1})	*n*	Cox (μmol)	Lag time (min)
TOP layer anaerobic respiration				
Endogenous	0.8 ± 0.4	4	0.42	0.00
Acetate	7.3 ± 1.0	4	2.48	0.25
Lactate	6.8 ± 0.7	4	3.72	0.25
Ethanol	5.5 ± 0.8	3	2.48	0.25
Glucose	3.9 ± 0.8	3	3.69	1.50
Xylose	3.7 ± 1.0	3	3.14	3.75
Mannose	3.7 ± 0.9	3	2.48	3.25
Site EPS	2.1 ± 0.5	4	0.72	3.25
D. autotrophicum EPS	0.3 ± 0.3	4	0.29	4.75
Xanthan	0.6 ± 0.3	4	0.29	4.75
Desulfovibrio EPS	1.5 ± 0.3	4	0.72	2.50

Table 3. Continued.

	$dH_2S/dt \pm SD$ ($\mu M\ min^{-1}$)	*n*	Cox (μmol)	Lag time (min)
Bottom layer aerobic respiration				
Endogenous	0.5 ± 0.2	4	0.34	0.00
Acetate	5.9 ± 1.7	4	2.48	0.00
Lactate	6.0 ± 2.8	4	3.72	0.25
Ethanol	6.0 ± 1.7	3	2.48	0.25
Glucose	3.5 ± 0.7	3	3.14	1.50
Xylose	3.7 ± 1.0	3	3.14	4.00
Mannose	3.6 ± 0.5	3	1.88	4.25
Site EPS	2.3 ± 1.1	4	0.68	3.00
D. autotrophicum EPS	0.3 ± 0.1	4	0.25	5.50
Xanthan	0.4 ± 0.3	4	0.25	5.00
Desulfovibrio EPS	1.4 ± 0.5	4	0.44	2.25

O_2 consumption represents aerobic respiration, and sulfide production is a measure of anaerobic respiration (Visscher *et al.*, 1998). The rate measurements upon substrate additions were corrected for the endogenous rates. Average rates ± 1 SD are given for the top (0–20 mm) and bottom (20–40 mm) layers of the mat. Cox represents the amount of carbon oxidized before the rates returned to endogenous values. Lag time represents the elapsed time between electron donor addition and start of oxygen uptake/sulfide production.

Site EPS was purified from the upper layer of the nonlithifying mat; *Desulfobacterium autotrophicum* and *Desulfovibrio* EPS (previously strain LM-1; Braissant *et al.*, 2007) were obtained from pure cultures of sulfate-reducing bacteria.

approximately five times lower than those of β-glucosidase, but showed a similar decrease at 2 cm depth (Fig. 6c). The depth profile of the β-galactosidase activity was very similar to that for α-glucosidase, with values between 10 and 4 $\mu mol\ g^{-1}\ h^{-1}$, but a steep decline in activity occurred at 3 cm depth (Fig. 6d).

Slurry experiments

After 24–36 h of incubation, endogenous rates were reduced to $< 10\%$ of the original values, and stimulation of metabolic rates upon addition of various carbon sources could be measured and corrected for the endogenous respiration rates. The potential aerobic respiration rates were similar in slurries prepared from the top and the bottom layers of the mat (Table 3). Sugar monomers (e.g. glucose, xylose, and mannose) stimulated aerobic respiration slightly more than LMW organic carbon (e.g. acetate, lactate, and ethanol), but the lag time before consumption commenced was shorter for the LMW organic compounds. The potential rates observed upon amendment of slurries with various types of EPS were much lower than for the other electron donors, but the values remained well above the endogenous rates. Likewise, the lag phase before consumption started was also the longest for the various types of EPS. The EPS obtained from nonlithifying mats in Salt Pan and an SRB isolate from this lake stimulated the aerobic respiration twice as much as did nonendogenous types of EPS (xanthan, *D. autotrophicum* EPS).

The combined action of fermenters and sulfate reducers was represented by the sulfide production (i.e. anaerobic respiration) rates. As observed in the aerobic rate measurements, the anaerobic respiration rates were also similar in the top and the bottom layer slurries. Potential anaerobic respiration rates were lower than potential aerobic rates (Table 3), even when considering that twice the amount of electron donor is used in sulfide production [Eqn. (2)] compared with oxygen consumption [Eqn. (1)]. In contrast to aerobic respiration, anaerobic slurries were stimulated more by LMW organic compounds (i.e. fermentation products) than by sugar monomers. The lag phase, before sugar and EPS consumption started, was longer in the anoxic slurry experiments than in the oxic incubations.

The amount of oxygen consumed and sulfide produced were used [Eqns (1) and (2), respectively] to determine the amount of carbon consumed upon addition of various electron donors (Table 3). We assumed an average carbon oxidation state of zero for acetate, lactate, sugar monomers, and EPS and an average carbon oxidation state of -2 for ethanol. LMW organic compounds were oxidized completely under both oxic and anoxic conditions. However, monomeric sugars were consumed completely only during aerobic respiration: in anaerobic respiration experiments, *c.* 40–50% remained when the rates returned to endogenous values. Interestingly, the amount of EPS-carbon oxidized under anoxic conditions was close to two-thirds of the amount used under oxic conditions. Estimates of the fraction of EPS readily supporting respiration were *c.* 8% and 5%, for aerobic and anaerobic consumption, respectively.

Carbonate mineral precipitation potential of EPS

$CaCO_3$ precipitated in all of the EPS solutions within 5 days, without the addition of calcium. Formation of bubbles was observed using light microscopy when HCl 0.1 N was added to the crystals, indicating their carbonate nature. Crystals formed in the top and the bottom layer EPS solutions had different morphologies (Fig. 7). Crystals produced in the top layer EPS consisted of mostly rounded, smoothed, and truncated rhombs measuring between 10 and 20 μm. Some spherulites were also found. In contrast, the bottom layer EPS produced only rhombohedra measuring between 5 and 10 μm.

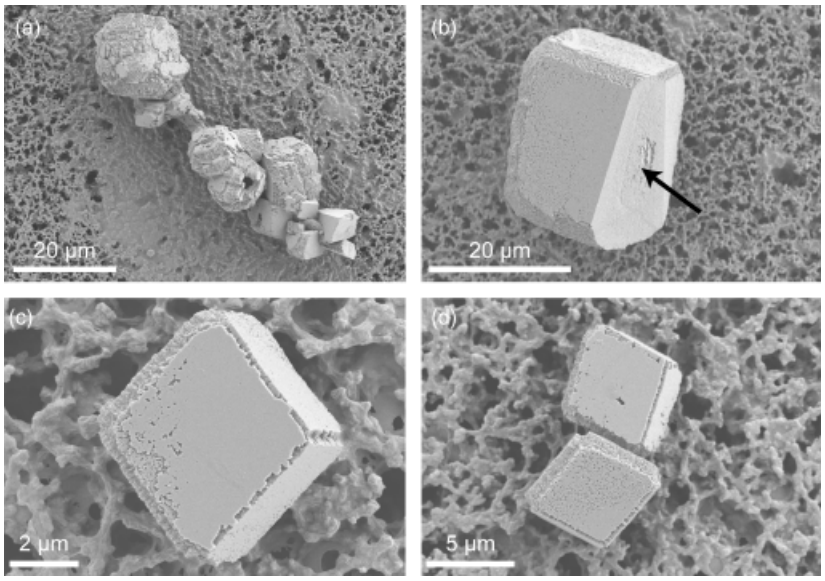

Fig. 7. SEM of carbonate crystals produced in the EPS during the biomineralization experiment. (a, b) Crystals produced in the top (0–20 mm) layer EPS. Arrow (b) indicating truncated edges, which is typical for a subhedral crystal shape. (c, d) Crystals produced in bottom layer EPS. These crystals exhibit rhombohedral and euhedral shapes.

Discussion

EPS in microbial mats are produced by a great variety of microorganisms (Stal *et al.*, 1985; Decho, 2000; Braissant *et al.*, 2007) in response to environmental cues, including salinity, UV irradiation, and desiccation (Decho, 1990; Potts, 1994; Wotton, 2004). However, the physicochemical properties of EPS play an additional and critical role in the long-term preservation of these communities by facilitating mineral precipitation (Trichet & Défarge, 1995). Carboxyl and other chemical functional groups bind cations, including calcium and magnesium, inhibiting calcium and/or magnesium carbonate precipitation in freshly produced EPS (Dupraz & Visscher, 2005; Braissant *et al.*, 2007). This inhibition is greatly reduced when EPS is altered through biotic or abiotic processes (Bosak, 2005; Wright & Wacey, 2005), leading to carbonate precipitation. Microbial activity is believed to be one of the main EPS-degrading processes (Dupraz & Visscher, 2005).

Our physicochemical characterizations clearly demonstrate that EPS abundances changed with depth. The most abundant polymers were associated with the upper 15 mm of the mat, which coincided with the green (i.e. cyanobacteria-rich) layer of the mat and with the maximum depth of oxygen penetration (Fig. 2), i.e. the potential aerobic respiration zone. Previously, it was shown that most of the sulfate-reducing activity was also associated with the top 10–12 mm of the nonlithifying mats of Salt Pan (Dupraz *et al.*, 2004). On comparing the values obtained with the Alcian Blue and phenol–sulfuric acid methods, the difference in abundance was roughly a factor of 2–3, which could be attributed to the differences in the EPS properties that were assayed. In the upper 15 mm of the mat, the phenol–sulfuric acid assay revealed a relatively constant amount of sugars in the EPS present, but the Alcian Blue assay showed that this EPS had an increased amount of acidic groups. The relatively constant abundance in depth horizons below 15 mm suggested that there was only minimal degradation of EPS below this point, indicating that this EPS was more refractory. A trend of changing EPS abundance with depth has been shown in other microbial mats as well (Mao Che *et al.*, 2001; Rougeaux *et al.*, 2001; Decho *et al.*, 2005).

In the present study, enzyme activities also mirrored changes in EPS properties with depth. The activities of reductase enzymes (TTC) peaked in the surface 10 mm of the mat (Fig. 6a), and rapidly declined below 20 mm. Reductase activities, linked to both aerobic and anaerobic respiration pathways and considered good proxies for total microbial metabolism (Fukui & Takii, 1989; McFeters *et al.*, 1995), were expected to decrease as microbial rates typically decrease with depth. We observed that the oxic zone penetrated down to *c.* 16–19 mm, which confirmed that the upper *c.* 20 mm was the most active part of the mat with respect to the production and consumption of oxygen. Other studies have shown that in nonlithifying mats, sulfate reduction rates also peak in the oxic zone near the surface (e.g. Canfield & DesMarais, 1991; Visscher *et al.*, 1992; Dupraz *et al.*, 2004; Casillas-Martinez *et al.*, 2005). Depth distributions of α- and β-glucosidases were the same as those of TTC, peaking in the top 10 mm of the mat and quickly decreasing below 20 mm (Fig. 6b and c). The β-glucosidic bonds are common in many biological polymers (Boetius, 1995; Sutherland, 1999). Therefore, it was not surprising to find a significant correlation between the β-glucosidase activity and the amount of EPS (Fig. 2) measured by the phenol–sulfuric acid assay ($r = 0.97$, $n = 8$, $P = 0.03$). The sharp decline of EPS, therefore, coincided with decreases in microbial activities as indicated by the

TTC assay, and also of specific enzymatic activities as indicated by the assays of hydrolytic enzymes. At depths >20 mm, there seemed to be less degradation of EPS and/or less new production of these polymers. However, the β-galactosidase activity declined more gradually and still showed substantial values at 20–30 mm depth. This could indicate that changes had occurred in the availability of sugars remaining within the EPS matrix.

Newly produced EPS at the surface of the mat supported high rates of microbial activity (Table 3, Fig. 6). Slurry-based observations provided further evidence that this surface EPS was labile: homogenized mats rapidly metabolized LMW organic molecules, sugars, and part of the amended EPS without novel induction of enzymes. Although compared with LMW organic compounds and sugar monomers, a slightly longer lag phase and slightly lower rates in mat slurries were observed upon addition of EPS from the site, the fresh polymers were rapidly turned over (i.e. within 20–30 min). Approximately 5–8% of the carbon present in the EPS was consumed during the incubation period before the rates leveled off to endogenous values. It should be emphasized that these rates were measured using mat homogenates and, therefore, were expected to be much higher than the turnover rates in intact mat systems (Visscher & van Gemerden, 1991; Visscher *et al.*, 1999). This may explain why this estimate is slightly higher than earlier observations using ^{14}C in stromatolite mats (Decho *et al.*, 2005). The EPS in deeper layers (> 30–40 mm) in the nonlithifying mats of Salt Pan, which coincided with strongly decreased microbial activities, were more refractory (Fig. 6).

Degradation of EPS likely consists of a multistep process representing sequential degradation of different EPS components, ranging from highly labile to relatively refractory, depending on their chemical composition and their steric availability to extracellular enzymes (Nankai *et al.*, 1999). As a consequence, these different EPS components have different relative rates of degradation. The present results showed that initial hydrolysis of EPS involved a rapid, and possibly selective, utilization by heterotrophs of certain EPS sugar monomers and LMW compounds. Typical sugar monomers in EPS include D-glucose, D-galactose, and D-mannose, and negatively charged uronic acids such as D-glucuronic acid and D-mannuronic acid (Sutherland, 2001b). Uronic acids and other monomers were shown to be highly labile to mat bacteria (Decho *et al.*, 2005). Chemical functional groups (e.g. carboxyl, phosphate, amine, and sulfate esters) on charged molecules, which could bind Ca^{2+} ions, are also present on LMW organic compounds such as pyruvic and acetic acids, or amino acids (e.g. L-glutamic acid, L-serine) on proteins (Sutherland, 2001b). Removal of charged monomers or LMW organic compounds will result in a net loss of functional groups on EPS, and potentially reduce their ability to complex Ca^{2+} and Mg^{2+} ions and inhibit precipitation. Small, charged proteins have been hypothesized to form complexes with polysaccharides, and act as a physical rebar to strengthen the EPS matrix (Flemming & Wingender, 2001). Removal of such proteins could influence the stability of EPS to further degradation or dissolution. Additionally, conformational changes in the EPS can change the ability of the polysaccharide itself to loosely bind cations through hydroxyl groups (Braccini *et al.*, 1999).

The EPS matrix of Salt Pan mats contained tightly bound calcium, whose amount remained fairly constant in the upper 40 mm. EPS that was dialyzed 10 times still contained calcium (Fig. 3). When additional calcium was added to this dialyzed EPS in our experiments, it was readily bound, but was released upon mild acidification (data not shown). This indicated that there were two different calcium pools: one loosely bound that could be exchanged by dialysis or by moderate changes in pH and one that was more tightly bound and was not exchanged. The presence of different calcium pools is in agreement with the current and previous observations that multiple functional groups, each with characteristic pK values, exist (Phoenix *et al.*, 2002; Braissant *et al.*, 2007). In future studies, we will assess the Ca-EPS binding by determining the apparent dissociation constant (K_d) at various pH values. Similar to the current observations, calcium was also strongly bound to cyanobacterial sheath material (i.e. EPS), and was not released, even when treated with 1 N HCl (Somers & Brown, 1978). It is possible that the more tightly bound calcium pool was involved in cross-linking EPS and was sterically protected. Alternatively, calcium binds to the various functional groups of newly produced EPS (Fig. 8, step 2). Next, this EPS-Ca could form the other half of its bidentate complex with LMW organic compounds (Fig. 8, steps 1–3). The resulting EPS-Ca-LMW organic carbon complex is highly labile and the LMW organic moiety could be readily removed by enzyme activity (Fig. 8, step 4, solid arrow), as was observed in our slurry experiments. Microbial oxidation of this LMW organic carbon yields inorganic carbon (CO_2/HCO_3^-) (Fig. 8, step 4, dotted arrow), increasing the saturation index and enabling $CaCO_3$ to precipitate (Fig. 8, step 5), assuming that the pH conditions allow for carbonate minerals' stability. Furthermore, if this LMW organic carbon was indeed the labile EPS fraction, then microbial removal would result in the formation of nucleation sites or 'pockets,' where early precipitation could occur. Finally, depending on the K_d of a specific functional group (i.e. 'A,' 'B' in Fig. 8) for the Ca-EPS, the $CaCO_3$ precipitate appears either associated with the EPS (Fig. 8, step 5: EPS-A-$CaCO_3$) or free in pockets within that matrix (Fig. 8, step 5: $CaCO_3$).

When nonlithifying mats were transplanted to the lithifying zone in Salt Pan, the calcium readily (i.e. within months) precipitated as a thin carbonate crust, most likely because of

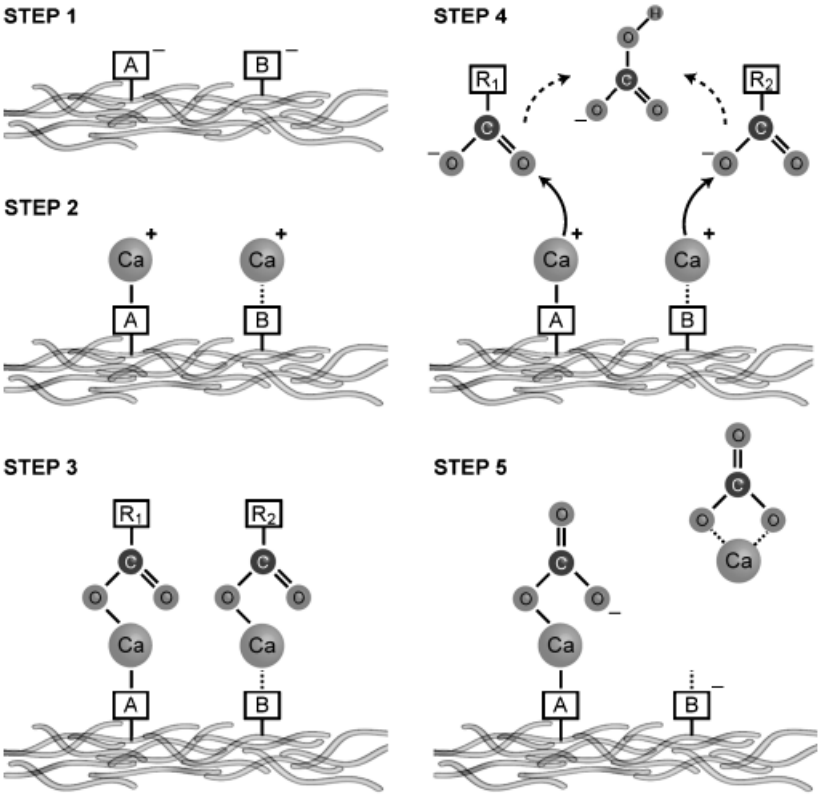

Fig. 8. Conceptual model of microbially mediated $CaCO_3$ precipitation in the EPS matrix. Step 1: functional groups (a, b) on EPS with different pK and K_d values for calcium exist; step 2: calcium binds either more or less tightly to functional groups A and B, respectively; step 3: LMW organic carbon and calcium on EPS form a bidentate complex; step 4: microbial activity removes LMW organic carbon (solid arrow), which is subsequently oxidized to bicarbonate (dashed arrow); step 5: the EPS–Ca complex binds carbonate. The $CaCO_3$ that is formed either remains linked to the EPS matrix (as EPS-A-$CaCO_3$) or exists freely in pockets within the EPS matrix.

increased microbial activity at the surface in the lithifying zone (C. Dupraz, pers. commun.). This corroborates the model proposed for Salt Pan (Dupraz *et al.*, 2004), in which the higher light conditions present in the lithifying zone stimulate cyanobacterial photosynthesis and, coupled to this, increased aerobic and anaerobic respiration rates (Dupraz *et al.*, 2004). Cyanobacterial production was linked to lithification in hypersaline mats at Lake La Chiprana, Spain (Jonkers *et al.*, 2003), and heterotrophic microbial activity was reported to be the likely mechanism for carbonate precipitation in the biofilm communities of open-water marine stromatolites, Bahamas (Reid *et al.*, 2000; Visscher *et al.*, 2000). The biomineralization experiment in the present study mimics the scenario of enhanced microbial activity increasing alkalinity and providing abundant carbonate ions within the EPS matrix in a purely chemical fashion [i.e. the decomposition of the $(NH_4)_2CO_3$ into CO_2 and NH_3 in the desiccator's atmosphere and the formation of carbonate ions in the EPS solution]. In addition, the pH increase induced by the NH_4^+/NH_3 system provides pH conditions similar to those found at the surface of a microbial mat during photosynthesis.

As outlined above, the sugar polymer scaffold of EPS contains a plethora of chemical functional groups as well as other molecules (Raguénès *et al.*, 1996; de Philippis *et al.*, 2001; Kawaguchi & Decho, 2002b; Braissant *et al.*, 2007). In the present study, the results of both FT-IR spectral analyses and acid–base titrations indicated that the chemical functional group composition changed with depth. This, coupled to the observed hydrolytic enzyme activities, suggested that the kerogenization process started at least in part through microbial activity. In this study, different minerals were precipitated in top vs. bottom layer EPS (Fig. 7). This was expected, as the Alcian Blue profile showed increased acidity with depth, and the acidity of the EPS affected the mineral composition and morphology of the $CaCO_3$ precipitate (Braissant *et al.*, 2003).

Although in rare cases EPS itself may be preserved in the rock record (Barbieri & Cavalazzi, 2004; Barbieri *et al.*, 2006), fossilization of microbial mats results predominantly from $CaCO_3$ precipitation. Microbial degradation of EPS produces HCO_3^-, increases the alkalinity, and reduces the quantity of cation-binding sites, releasing cations such as Ca^{2+} and Mg^{2+}. Furthermore, degradation of EPS provides the necessary nucleation sites for mineral precipitation (Figs 6 and 8). However, it is highly likely that EPS is also continuously produced (e.g. by SRB; Asaulenko *et al.*, 2004; Braissant *et al.*, 2007); the precipitation of carbonate minerals seems to be controlled by a balance between EPS production and degradation. In microbial mats, EPS can be considered as a calcium reservoir; therefore, its new production will increase the pool of calcium in the mat. In contrast (partial) EPS degradation will release calcium locally, thus allowing nucleation and precipitation of carbonate

minerals. This scenario is similar to that outlined for the Bahamian hypersaline mats and to calcification within a Polynesian microbial mat attributed to EPS degradation through loss of protein-associated carboxylic acids (Sprachta *et al.*, 2001; Gautret *et al.*, 2004). In addition to heterotrophic bacteria, fungi, such as isolates from hypersaline, EPS-rich mats (Cantrell *et al.*, 2006), could play an important role in the hydrolysis of EPS.

The microbial degradation of EPS undoubtedly plays a pivotal role in mineral precipitation. However, abiotic alterations of EPS should also be considered. These may include UV irradiation, photochemically produced superoxide radicals, ionic changes (i.e. salinity), and elevated temperatures. Future studies need to address the synergistic and antagonistic effects of both physicochemical and biological EPS degradation to fully understand the mechanism of $CaCO_3$ precipitation. This may provide the link between modern microbial mats and their fossil counterparts in the rock record.

Acknowledgements

This work was supported by NSF EAR 0221796 and NSF EAR 0331929 awarded to Pieter Visscher and SNF project funding no. 108141 awarded to Christophe Dupraz. Olivier Braissant thanks the Swiss National Fund for the postdoctoral fellowship grant PBNEA-110305 that sponsored a visit to UConn, The 'Société Académique Vaudoise' that sponsored XPS time, and Eric P. Verrecchia for his support. This is contribution #14 of UConn's Center for Integrative Geosciences.

References

Anderson KL, Tayne TA & Ward DA (1987) Formation and fate of fermentation products in hot spring cyanobacterial mats. *Appl Environ Microb* **53**: 2343–2352.

Asaulenko LH, Purishch LM & Kozlova IP (2004) Stages of biofilm formation by sulfate-reducing bacteria. *Mikrobiologiya* **66**: 72–79.

Barbieri R & Cavalazzi B (2004) Microbial fabrics from Neogene cold seep carbonates, Northern Apennine, Italy. *Palaeontology* **227**: 143–155.

Barbieri R, Stivaletta N, Marinangeli L & Ori GG (2006) Microbial signatures in sabkha evaporite deposits of Chott el Gharsa (Tunesia) and their astrobiological implications. *Planet Space Sci* **54**: 726–736.

Battersby NS, Stewart DJ & Sharma AP (1984) Effect of Xanthan on the growth of sulfate-reducing bacteria in marine sediments. In *Deuxième Colloque International de Bactériologie marine*. CNRS, Brest, octobre 1–5, 1984: IFREMER.

Baumgartner LK (2006) Diversity and lithification in microbial and stromatolites. PhD Thesis, University of Connecticut, Marines Sciences, Groton.

Baumgartner LK, Reid RP, Dupraz C, Decho AW, Buckley DH, Spear JR, Przekop KM & Visscher PT (2006) Sulfate-reducing bacteria in microbial mats: changing paradigms, new discoveries. *Sediment Geol* **185**: 131–145.

Bober C, Mojica K & Cooney M (2005) Quantification of single-species marine biofilm with Alcian Blue. *J Young Investigator* **12**: 1–7.

Boetius A (1995) Microbial hydrolytic enzyme activities in deep sea sediments. *Helgolander Meersun* **49**: 177–187.

Bosak T (2005) Laboratory models of microbial biosignatures in carbonate rocks. PhD Thesis, California Institute of Technology, Pasadena, CA.

Braccini I, Grasso RP & Pérez S (1999) Conformational and configurational features of polysaccharides and their interactions with calcium a molecular modeling investigation. *Carbohyd Res* **317**: 119–130.

Braissant O, Cailleau G, Dupraz C & Verrecchia EP (2003) Bacterially induced mineralization of calcium carbonate in terrestrial environments: the role of exopolysaccharides and amino acids. *J Sediment Res* **73**: 485–490.

Braissant O, Decho AW, Dupraz C, Glunk C, Przekop KM & Visscher PT (2007) Exopolymeric substances of sulfate-reducing bacteria: interactions with calcium at alkaline pH and implication for formation of carbonate minerals. *Geobiology* **5**: 401–411.

Canfield DE & DesMarais DJ (1991) Aerobic sulfate reduction in microbial mats. *Science* **251**: 1471–1473.

Cantrell SA, Casillas L & Molina M (2006) Characterization of fungi from hypersaline environments of solar salterns using morphological and molecular techniques. *Mycol Res* **110**: 962–970.

Casillas-Martinez L, Gonzalez ML, Fuentes Z, Nieves D, Hernandez C, Ramirez W, Sytsma RE, Perez-Jimenez J & Visscher PT (2005) Community structure, geochemical characteristics and mineralogy of a hypersaline microbial mat, Cabo Rojo, PR. *Geomicrobiol J* **22**: 269–281.

Coates J (2000) Interpretation of infrared spectra, a practical approach. *Encyclopedia of Analytical chemistry* (Meyers RA, ed), pp. 10815–10837. John Wiley and Sons Ltd, Chichester.

Costerton JW, Cheng KJ, Geesey GG, Ladd TI, Nickel JC, Dasgupta M & Marrie TJ (1987) Bacterial biofilms in nature and disease. *Annu Rev Microbiol* **41**: 435–464.

Costerton JW, Lewandowski Z, Caldwell DE, Korber DR & Lappin-Scott HM (1995) Microbial biofilms. *Annu Rev Microbiol* **49**: 711–745.

Decho AW (1990) Microbial exopolymer secretions in ocean environments: their role(s) in food webs and marine processes. *Oceanogr Mar Biol Annu Rev* **28**: 73–154.

Decho AW (2000) Microbial biofilms in intertidal systems: an overview. *Cont Shelf Res* **20**: 1257–1273.

Decho AW, Kawaguchi T, Allison MA, Louchard EM, Reid RP, Stephens FC, Voss KJ, Wheatcroft RA & Taylor BB (2003) Sediment properties influencing upwelling spectral reflectance signatures: the 'Biofilm gel effect'. *Limnol Oceanogr* **48**: 431–443.

Decho AW, Visscher PT & Reid RP (2005) Production and cycling of natural microbial exopolymers (EPS) within a marine stromatolite. *Palaeontology* **219**: 71–86.

de Philippis R, Sili C, Paperi R & Vincenzini M (2001) Exopolysaccharide-producing cyanobacteria and their possible exploitation: a review. *J Appl Phycol* **13**: 293–299.

Dubois M, Gilles KA, Hamilton JK, Rebers PA & Smith F (1956) Colorimetric method for determination of sugars and related substances. *Anal Chem* **28**: 350–356.

Dupraz C & Visscher PT (2005) Microbial lithification in marine stromatolites and hypersaline mats. *Trends Microbiol* **13**: 429–438.

Dupraz C, Visscher PT, Baumgartner LK & Reid RP (2004) Microbe-mineral interactions: early carbonate precipitation in a hypersaline lake (Eleuthera Island, Bahamas). *Sedimentology* **51**: 745–765.

Ercole C, Cacchio P, Botta AL, Centi V & Lepidi A (2007) Bacterially induced mineralization of calcium carbonate: the role of exopolysaccharides and capsular polysaccharides. *Microscop Microanal* **13**: 42–50.

Flemming HC & Wingender J (2001) Relevance of microbial extracellular polymeric substances (EPS) – part I: structural and ecological aspects. *Water Sci Technol* **43**: 1–8.

Fukui M & Takii S (1989) Reduction of tetrazolium salts by sulfite-reducing bacteria. *FEMS Microbiol Ecol* **62**: 13–20.

Gautret P, Camoin G, Golubic S & Sprachta S (2004) Biochemical control of calcium carbonate precipitation in modern lagoonal microbialites, Tikehau atoll, French Polynesia. *J Sediment Res* **74**: 462–464.

Hashimoto W, Miki H, Tsuchiya N, Nankai H & Murata K (1998) Xanthan lyase of *Bacillus* sp. strain GL1 liberates pyruvylated mannose from xanthan side chains. *Appl Environ Microb* **64**: 3765–3768.

Henrichs SM & Doyle AP (1986) Decomposition of ^{14}C-labeled organic substances in marine sediments. *Limnol Oceanogr* **31**: 765–778.

Jonkers HM, Ludwig R, de Wit R, Pringault O, Muyzer G, Niemann H, Finke N & de Beer D (2003) Structural and functional analysis of a microbial mat ecosystem from a unique permanent hypersaline inland lake: 'La Salada de Chiprana' (NE Spain). *FEMS Microbiol Ecol* **44**: 175–189.

Kawaguchi T & Decho AW (2002a) A laboratory investigation of cyanobacterial extracellular polymeric secretions (EPS) in influencing $CaCO_3$ polymorphism. *J Cryst Growth* **240**: 230–235.

Kawaguchi T & Decho AW (2002b) Isolation and biochemical characterization of extracellular polymeric secretions (EPS) from modern soft marine stromatolites (Bahamas) and its inhibitory effect on $CaCO_3$ precipitation. *Prep BioChem Biotech* **32**: 51–63.

Mao Che L, Andréfouët S, Bothorel V *et al.* (2001) Physical, chemical, and microbiological characteristics of microbial mats (KOPARA) in the south Pacific atolls of French Polynesia. *Can J Microbiol* **47**: 944–1012.

McFeters GA, Yu FP, Pyle BH & Stewart PS (1995) Physiological assessment of bacteria using fluorochromes. *J Microbiol Meth* **21**: 1–13.

Nankai H, Hashimoto W, Miki I, Kawai S & Murata K (1999) Microbial system for polysaccharide depolymerization: enzymatic route for xanthan depolymerization by *Bacillus* sp. strain GL1. *Appl Environ Microb* **65**: 2520–2526.

Noffke N, Hazen R & Nhleko N (2003) Earth's earliest microbial mats in a siliciclastic marine environment (2.9 Ga Mozaan Group, South Africa). *Geology* **31**: 673–676.

Omoike A & Chorover J (2004) Spectroscopic study of extracellular polymeric substances from *Bacillus subtilis*: aqueous chemistry and adsorption effects. *Biomacromolecules* **5**: 1219–1230.

Ortega-Morales BO, Santiago-Garcia JL, Chan-Bacab MJ, Moppert X, Miranda-Tello E, Fardeau ML, Carrero JC, Bartolo-Pérez P, Valadéz-Gonzalez A & Guezennec J (2007) Characterization of extracellular polymers synthesized by tropical intertidal biofilm bacteria. *J Appl Microb* **102**: 254–264.

Paerl HW, Steppe TF & Reid RP (2001) Bacterially-mediated precipitation in marine stromatolites. *Environ Microbiol* **3**: 123–130.

Passow U & Alldredge AL (1995) A dye-binding assay for the spectrophotometric measurement of transparent exopolymer particles (TEP). *Limnol Oceanogr* **40**: 1326–1335.

Perry TD IV, Klepac-Ceraj V, Zhang XV, McNamara CJ, Polz MF, Martin ST, Berke N & Mitchell R (2005) Binding of harvested bacterial exopolymers to the surface of calcite. *Environ Sci Technol* **39**: 8770–8775.

Phoenix VR, Martinez RE, Konhauser KO & Ferris FG (2002) Characterization and implications of the cell surface reactivity of *Calothrix* sp. strain KC97. *Appl Environ Microb* **68**: 4827–4834.

Potts M (1994) Desiccation tolerance of prokaryotes. *Microbiol Rev* **58**: 755–805.

Raguénès G, Pignet P, Gauthier G, Peres A, Christen R, Rougeaux H, Barbier G & Guezennec J (1996) Description of a new polymer-secreting bacterium from a deep-sea hydrothermal vent, *Alteromonas macleodii* subsp. *fijiensis*, and preliminary characterization of the polymer. *Appl Environ Microb* **62**: 67–73.

Raguénès G, Moppert X, Richert L, Ratiskol J, Payri C, Costa B & Guezennec J (2004) A Novel exopolymer-producing bacterium, *Paracoccus zeaxanthinifaciens* subsp. *payriae*, isolated from a "Kopara" mat located in Rangiroa, an atoll of French Polynesia. *Curr Microbiol* **49**: 145–151.

Reid RP, Visscher PT, Decho AW *et al.* (2000) The role of microbes in accretion, lamination and early lithification of modern marine stromatolites. *Nature* **406**: 991–992.

Relexans JC (1996) Measurements of the respiratory electron transport system (ETS) activity in marine sediments: state-of-the-art and interpretation. I. Methodology and review of the literature data. *Mar Ecol Prog Ser* **136**: 277–287.

Riding RE & Awramik SM (2000) *Microbial Sediments*. Springer-Verlag, Heidelberg.

Rougeaux H, Guezennec M, Mao Che L, Payri P, Deslandes E & Guezennec J (2001) Microbial communities and exopolysaccharides from polynesian mats. *Mar Biotechnol* **3**: 181–187.

Schiewer S (1999) Modelling complexation and electrostatic attraction in heavy metal biosorption by Sargassum biomass. *J Appl Phycol* **11**: 79–87.

Shimomura O & Inouye S (1996) Titration of recombinant aequorin with calcium chloride. *Biochem Biophysl Res Commun* **221**: 77–81.

Smith BC (1996) *Fundamentals of Fourier Transform Infrared Spectroscopy*. CRC Press, Boca Raton.

Smith PK, Krohn RI, Hermanson GT, Mallia AK, Gartner FH, Provenzano MD, Fujimoto EK, Goecke NM, Olson BJ & Klenk DC (1985) Measurement of protein using bicinchoninic acid. *Anal Biochem* **150**: 76–85.

Socrates G (2001) *Infrared and Raman Characteristic Group Frequencies: Tables and Charts*. Wiley, New York.

Somers GF & Brown M (1978) The affinity of trichomes of blue-green algae for calcium ions. *Estuaries* **1**: 17–28.

Sprachta S, Camoin G, Golubic S & Le Campion T (2001) Microbialites in a modern lagoonal environment: nature and distribution, Tikehau atoll (French Polynesia). *Palaeontology* **175**: 103–124.

Stal LJ, van Gemerden H & Krumbein WE (1985) Structure and development of a benthic microbial mat. *FEMS Microbiol Ecol* **31**: 111–125.

Stolle-Smits T, Beekhuizen JG, Kok MTC, Pijnenburg M, Recourt K, Derksen J & Voragen AGJ (1999) Changes in cell wall polysaccharides of green bean pods during development. *Plant Physiol* **121**: 363–372.

Stolz JF (2000) Structure of microbial mats and biofilms. *Microbial Sediments* (Riding RE & Awramik SM, eds), pp. 1–8. Springer-Verlag, Heidelberg.

Stumm W & Morgan JJ (1996) *Aquatic Chemistry*. John Wiley & Sons Inc., New York.

Sutherland IA (1995) Polysaccharide lyases. *FEMS Microbiol Rev* **16**: 323–347.

Sutherland IA (1999) Polysaccharases for microbial exopolysaccharides. *Carbohyd Polym* **38**: 319–328.

Sutherland IA (2001a) The biofilm matrix – an immobilized but dynamic microbial environment. *Trends Micorbiol* **9**: 222–227.

Sutherland IA (2001b) Biofilm exopolysaccharides: a strong and sticky framework. *Microbiology* **147**: 3–9.

Sutherland IA (2001c) Exopolysaccharides in biofilms, floc and realated structures. *Wat Sci Technol* **43**: 77–86.

Sutherland IA (2001d) Microbial polysaccharides from Gram-negative bacteria. *Int Dairy Journal* **11**: 663–674.

Tice M (2008) Modern life in ancient mats. *Nature* **452**: 40–41.

Trichet J & Défarge C (1995) Non-biologically supported organomineralization. *BI Oceanogr Monaco* **14** (special issue): 203–226.

Troelsen H & Jørgensen BB (1982) Seasonal dynamics of elemental sulfur in two coastal sediments. *Estuar Coast Shelf S* **15**: 255–266.

Turner BF & Fein JB (2006) Protofit: a program for determining surface protonation constants from titration data. *Comput Geosci* **32**: 1344–1356.

Visscher P, Reid RP & Bebout BM (2000) Microscale observations of sulfate reduction: correlation of microbial activity with lithified micritic laminae in modern marine stromatolites. *Geology* **28**: 919–922.

Visscher PT & van Gemerden H (1991) Production and consumption of dimethyl-sulfoniopropionate in marine microbial mats. *Appl Environ Microb* **57**: 3237–3242.

Visscher PT, Beukema J & van Gemerden H (1991) In situ characterization of sediments: measurements of oxygen and sulfide profiles. *Limnol Oceanogr* **36**: 1476–1480.

Visscher PT, Prins RA & van Gemerden H (1992) Rates of sulfate reduction and thiosulfate consumption in a marine microbial mat. *FEMS Microbiol Ecol* **86**: 283–294.

Visscher PT, Reid RP, Bebout BM, Hoeft SE, Macintyre IG & Thompson JA (1998) Formation of lithified micritic laminae in modern marine stromatolites (Bahamas): the role of sulfur cycling. *Am Mineral* **83**: 1482–1493.

Visscher PT, Gritzer RF & Leadbetter ER (1999) Low-molecular-weight sulfonates, a major substrate for sulfate reducers in marine microbial mats. *Appl Environ Microb* **65**: 3272–3278.

Visscher PT, Surgeon TM, Hoeft SE, Bebout BM, Thompson J Jr & Reid RP (2002) Microelectrode studies in modern marine stromatolites: unraveling the earth's past? *Environmental Electrochemistry: Analyses of Trace Element Biogeochemistry. American Chemical Society Symposium Series 811* (Taillefert M & Rozan T, eds), pp. 265–282. Oxford University Press, New York.

Weaver DT & Hicks RE (1995) Biodegradation of *Azotobacter vinelandii* exopolymer by lake Superior microbes. *Limnol Oceanogr* **40**: 1035–1041.

Wotton RS (2004) The ubiquity and many roles of exopolymers (EPS) in aquatic systems. *Sci Mar* **68**: 13–21.

Wright DT & Wacey D (2005) Precipitation of dolomite using sulphate-reducing bacteria from the Coorong Region, South Australia: significance and implications. *Sedimentology* **52**: 987–1008.